EXCITATION OF DISCRETE ALFVEN WAVES IN TOKAMAKS

K. Appert, R. Gruber, F. Troyon and J. Vaclavik

Centre de Recherches en Physique des Plasmas
Association Euratom - Confédération Suisse
Ecole Polytechnique Fédérale de Lausanne
CH-1007 Lausanne / Switzerland

ABSTRACT

Analytical and numerical demonstrations of the existence of discrete Alfvén modes are presented. Possible implications for a low frequency heating of Tokamaks are discussed.

1. INTRODUCTION

Recent experimental (de Chambrier et al., 1981) and numerical (Ross et al., 1981) results concerning the antenna loading for the Alfvén wave heating of Tokamak plasmas show the evidence of resonant peaks at frequencies just below the lower edge of the Alfvén continuum. A similar peak has been noticed in the calculations of MHD spectrum by Pochelon et al. (1975). The objective of this paper is to provide a simple interpretation of these phenomena by means of the ideal MHD theory. In particular, we shall show that the resonant peaks can be related to the excitation of a new type of waves which we propose to call "discrete Alfvén waves". Also we discuss a possibility to use these modes for a "Discrete Alfvén Resonance Heating" (DARH) scheme of Tokamak plasmas.

The plan of the paper is now outlined. In Section 2 the Hain-Lüst equation is used as a basic equation for the ideal MHD model in cylindrical geometry, together with a short discussion of the continuous spectrum. In Section 3 we show, for a low-β plasma, the existence of discrete Alfvén modes by means of a WKB approach and through numerical calculations performed using our one-dimensional stability code THALIA (Appert et al., 1975). In Section 4 we present analytical calculations which predict that, under some circumstances, the lower edge of the Alfvén continuum is an accumulation point of the discrete Alfvén modes. Section 5 deals with the effects of toricity. Finally, in Section 6 we put forward some ideas about using these modes for a low frequency heating of tokamaks.

2. BASIC EQUATIONS AND CONTINUOUS SPECTRUM

A circular cross-section Tokamak with the large aspect ratio R_a can be considered as a straight cylindrical plasma column with the usual correspondance $k = n/R_a$ between the longitudinal (z-direction) wavenumber k and the toroidal wavenumber n. Denoting by m the azimuthal (θ-direction) wavenumber, the linear displacement vector $\underline{\xi} = (\xi_r, \xi_\theta, \xi_z)$ can be Fourier-analysed in time, θ and z:

$$\underline{\xi}(t, r, \theta, z) = \underline{\xi}(r) \exp\left[i(\omega t + m\theta + kz)\right], \qquad (1)$$

where r is the remaining independent radial variable. In the ideal MHD model, the eigenfrequency ω and the eigenmode $\underline{\xi}(r)$ are obtained by solving the Hain-Lüst equation (Hain and Lüst, 1958)

$$\frac{d}{dr}\left[\frac{D}{N}\frac{1}{r}\frac{d}{dr}(r\xi_r)\right] + \left[A - \frac{d}{dr}\left(\frac{B_\theta}{r}\right)^2 - \frac{4k^2B_\theta^2(\rho\omega^2B^2 - \gamma pF^2)}{r^2N} + r\frac{d}{dr}\left(\frac{2kB_\theta GS}{r^2N}\right)\right]\xi_r = 0, \qquad (2)$$

where

$$D = AS \equiv [\rho\omega^2 - F^2][\rho\omega^2(\gamma p + B^2) - \gamma pF^2],$$

$$F = \underline{k}\cdot\underline{B} \equiv kB_z + \frac{m}{r}B_\theta,$$

$$G = \underline{k}\times\underline{B} \equiv \frac{m}{r}B_z - kB_\theta,$$

$$N = \rho\omega^2(A - G^2) - \gamma p\left(\frac{m^2}{r^2} + k^2\right)A .$$

The quantities $\underline{B} = (0, B_\theta, B_z)$, p, ρ and γ are the equilibrium magnetic field, the equilibrium pressure, the mass density and the specific heat ratio, respectively. The plasma is surrounded by a vacuum region which is limited by a concentric wall.

For given n (or k) and m, the MHD spectrum contains two continua (Appert et al., 1974) defined by D = 0. The slow wave continuum is given by

$$\omega_s^2 = \frac{\gamma p F^2}{\rho(\gamma p + B^2)} \tag{3}$$

and the Alfvén continuum by

$$\omega_A^2 = F^2/\rho \quad . \tag{4}$$

The frequency range of the Alfvén continuum is

$$Min\left[\omega_A^2(r)\right] \leq \omega^2 \leq Max\left[\omega_A^2(r)\right]. \tag{5}$$

It is well known that besides these continua there are discrete modes. In particular, all unstable modes are discrete. Also discrete are the fast modes with an accumulation point at $\omega = \infty$.

An example of the extension of the Alfvén continuum as a function of n is shown in Fig. 1. The curves corresponding to the Alfvén fre-

quencies at the axis ($\omega_A^2(0)$) and the plasma surface ($\omega_A^2(1)$) are drawn as solid lines. The dotted lines represent the lower limit of the Alfvén continuum corresponding to the local Alfvén frequency somewhere inside the plasma. At this point we have

$$\frac{d\,\omega_A^2}{dr} = 0, \tag{6}$$

whereas at $r = 0$ and $n = n_c$

$$\frac{d\,\omega_A^2}{dr} = \frac{d^2\omega_A^2}{dr^2} = \frac{d^3\omega_A^2}{dr^3} = 0. \tag{7}$$

3. DISCRETE ALFVEN MODES

The recent experimental results obtained on the TCA Tokamak at Lausanne (de Chambrier et al., 1981) and the numerical results obtained by Ross et al. (1981) suggest the existence of one or more weakly-damped eigenmodes at frequencies just below the lower edge of the Alfvén continuum. At the first glance, this is a surprising finding. However, a simple inspection of the equation (2) may already shed some light on the phenomenon. Indeed, on performing a WKB-type of analysis of this equation one finds a seemingly-new type of waves whose dispersion relation reads

$$\omega^2 = \omega_A^2 - \frac{C}{k_r^2}\,, \tag{8}$$

where

$$C = \frac{G^2}{\rho B^2}\left\{\frac{4B_\theta^4}{r^2B^2(1-H)^2} + r\frac{d}{dr}\left[\frac{B_\theta^2(1+H)}{r^2(1-H)}\right]\right\}, \qquad (9)$$

$$H = \frac{FB_z}{kB^2}$$

and k_r is the radial wavenumber. These waves may be called the discrete Alfvén waves. They can easily be found by our one-dimensional spectral code THALIA (Appert et al., 1975) which, in principle, solves equation (2). In order not to be bothered by the slow wave continuum we compress it to $\omega = 0$ by setting $\gamma = 0$, which is a good approximation for low-β plasmas. The eigenmodes then satisfy $\underline{\xi} \cdot \underline{B} = 0$ with a motion purely perpendicular to the magnetic field. As to the current and density profiles we choose

$$j_\theta = 0\,, \quad j_z = j_0\left(1-r^2\right)^{\kappa_j},$$
$$\rho = \rho_0\left[(1-\Delta)\left(1-r^2\right)^{\kappa_\rho} + \Delta\right], \qquad (10)$$

which represent a good parametrization of ohmically-heated Tokamaks. The exponents κ_j and κ_ρ are free parameters. In nowadays Tokamaks the current seems to be more peaked than the density with κ_j larger than κ_ρ. The constant j_0 is determined such that the safety factor at the axis $q_0 = B_z r/RB_\theta = 1$. The density at the axis ρ_0 appears only in the normalizing Alfvén frequency ω_N (units are chosen

such that $\mu_0 = 1$ and the plasma radius = 1)

$$\omega_N^2 = \frac{B_z^2}{\rho_0} \quad . \tag{11}$$

The parameter Δ defines a pedestal of the density. If it equals zero, the Alfvén continuum extends to ∞. The quantity n_c can now easily be calculated

$$n_c = m\left[\frac{\kappa_j}{\kappa_\rho(1-\Delta)} - 1\right]. \tag{12}$$

We choose, as the standard case, the following values of the parameters

$$\begin{aligned} \kappa_j &= 4, \quad \kappa_\rho = 1, \\ B_z &= 1, \quad \Delta = .05, \\ m &= 1, \quad \rho_0 = 1, \end{aligned} \tag{13}$$

which yields $n_c = 3.2105$.

In Fig. 2 we show the discrete Alfvén modes in the stable region. The distance $\Delta\omega^2$ of these modes from the lower edge of the Alfvén continuum is plotted as a function of n. Only the modes with $\Delta\omega^2 > 10^{-5}$ are given. At $n = n_c$ (marked by II) we find 13 discrete modes. The number of the discrete Alfvén modes decreases for $n < n_c$ (region I) and for $n > n_c$ (region III). For high n ($n > 7$) all discrete modes seem to disappear. For negative n numbers, the

uppermost kink-like mode becomes unstable and the other discrete modes disappear.

The high density of the discrete modes at $n = n_c$ is demonstrated in Fig. 3. At this point 19 discrete Alfvén modes have been found when using 100 radial intervals and accumulating the mesh at the axis. Additional 81 Alfvén modes lie in the continuous part of this class of eigenmodes. The distance $\Delta\omega^2$ is plotted versus the radial mode number ℓ. For $\ell > 10$ we find a $1/\ell^4$ dependence of $\Delta\omega^2$. In the regions I and III the relative distance between the modes with different radial mode numbers is much larger. The spacing increases when the distance from the point $n = n_c$ increases.

The eigenmodes corresponding to three different values of n are displayed in Fig. 4. For $n = 2$ we find four discrete eigenmodes in the region I (Fig. 4a). The character of these modes show a localization around the radial position $r = r_c$ at which $d\omega_A^2/dr = 0$. In Fig. 4b the first six discrete eigenmodes are shown for $n = n_c$ (II). These modes are localized more and more at the axis. Even stronger localization at the axis is seen when plotting, in Fig. 4c, the four discrete eigenmodes found for $n = 4$ (region III).

We now turn to study these phenomena analytically.

4. ANALYTICAL INVESTIGATION OF THE DISCRETE ALFVEN MODES

The three regions defined above are treated separately. They are characterized by

I: $(\omega_A^2)' = 0$ and $(\omega_A^2)'' > 0$ at $r = r_c \neq 0$

II: $(\omega_A^2)' = (\omega_A^2)'' = (\omega_A^2)''' = 0$ and $(\omega_A^2)^{IV} > 0$ at $r = 0$

III: $(\omega_A^2)' = 0$ and $(\omega_A^2)'' > 0$ ar $r = 0$

Let us investigate each region:

(a) Region I

In this region the analytical treatment is very similar to the Suydam (1958) or Newcomb (1960) theory. The existence of discrete modes with eigenvalues ω^2 below the lower edge of the continuum is related to the behaviour of the solutions of the Hain-Lüst equation around $\omega^2 = \mathrm{Min}(\omega_A{}^2(r))$. In particular, the edge of the continuum is an accumulation point of a discrete spectrum if the singular solution has an oscillatory singularity at $r = r_c$. To treat this case we have to expand $\omega^2 - \omega_A{}^2$ around $\mathrm{Min}(\omega_A{}^2(r))$:

$$A/\rho = \omega^2 - \omega_A^2 \cong -\frac{1}{2}(\omega_A^2)''(r-r_c)^2 \equiv -\frac{1}{2}(\omega_A^2)'' x^2. \qquad (14)$$

Setting $\gamma = 0$ we find the following reduced Hain-Lüst equation which is valid around $r = r_c$:

$$x^2 \xi_r'' + 2x \xi_r' + g_I(r_c) \xi_r = 0 , \tag{15}$$

where

$$g_I = -2C/(\omega_A^2)'' . \tag{16}$$

Assuming $\xi_r \sim x^\alpha$ one obtains a characteristic polynomial which indicates that oscillatory solutions are present if

$$g_I - \frac{1}{4} > 0 . \tag{17}$$

For our standard case (see Eq. 13) we find

$$\begin{aligned} g_I - \tfrac{1}{4} > 0 \quad &\text{for} \quad 0 \le r < .92 \quad \text{or} \quad n_c \gtrsim n > -.12 , \\ g_I - \tfrac{1}{4} < 0 \quad &\text{for} \quad .92 < r \le 1 \quad \text{or} \quad -.12 > n > -.18 . \end{aligned} \tag{18}$$

This shows that there is an accumulation point in the region $-.12 < n \lesssim n_c$ (see Fig. 2). The density of the modes in the vicinity of the accumulation point can be estimated by means of the same type of calculations as that used by Pao (1974) for the Suydam modes. It yields

$$\Delta\omega^2 \sim \exp\left[-\text{const}\left(g_I - \frac{1}{4}\right)^{-1/2}\right] . \tag{19}$$

This behaviour is in accordance with the numerical results shown in Fig. 2. At $n = -.12$, $g_I - 1/4 = 0$ and the distance between the modes close to the accumulation point goes to zero. Numerically, we only find two discrete modes. With increasing n, $g_I - 1/4$ increases and becomes infinite at $n = n_c$, which leads to a different asymptotic behaviour. Numerically, the number of discrete modes also increases with increasing n.

(b) Essential singularity (II)

At the point $n = n_c$, the first three derivatives of ω_A^2 are equal to zero. A is then expanded around $r = 0$:

$$A/\varsigma = \omega^2 - \omega_A^2 \cong -\frac{1}{4!}(\omega_A^2)^{IV} r^4 . \tag{20}$$

The reduced Hain-Lüst equation then reads

$$r^4 \xi_r'' + 7r^3 \xi_r' + g_{II}(r=0)\,\xi_r = 0, \tag{21}$$

where

$$g_{II} = -24C/(\omega_A^2)^{IV} . \tag{22}$$

By virtue of a WKB analysis we can estimate the eigenvalues close to the accumulation point:

$$\Delta\omega^2 \sim (\omega_A^2)^{IV} g_{II}^2 / \ell^4 . \tag{23}$$

We find the same $1/\ell^4$-dependence as in Fig. 3.

(c) Region III

In this region A is again expanded around r = 0

$$A/\rho = \omega^2 - \omega_A^2 \cong -\frac{1}{2}(\omega_A^2)'' r^2. \tag{24}$$

The reduced Hain-Lüst equation then becomes

$$r^2 \xi_r'' + 5r\xi_r' + g_{III}(r=0)\,\xi_r = 0, \tag{25}$$

where

$$g_{III} = 3 - m^2 - \frac{2C}{(\omega_A^2)''} \quad . \tag{26}$$

Setting $\xi \sim r^\alpha$ one finds a characteristic polynomial which indicates that oscillatory solutions exist if

$$g_{III} - 4 > 0. \tag{27}$$

In our standard case this criterion is satisfied in the region $n_c \leq n < 7.28$. The density of the modes in the vicinity of the accumulation point can again be estimated by means of Pao's theory giving, similarly to region I (see Eq. 19),

$$\Delta\omega^2 \sim \exp\left[-\text{const}\left(g_{III} - 4\right)^{-1/2}\right]. \qquad (28)$$

Again this behaviour is in accordance with the numerical results shown in Fig. 2. At $n = 7.28$, $g_{III} - 4 = 0$ and the distance between modes close to the accumulation point tends to zero. Numerically, we cannot resolve a density of the modes which is too high and we only see the first discrete mode around $n = 7$. With decreasing n, $g_{III} - 4$ increases and becomes infinite at $n = n_c$, which leads again to the asymptotic behaviour discussed earlier (essential singularity). Numerically, more and more discrete modes are found when we approach $n = n_c$.

5. DISCRETE ALFVEN MODES IN TOROIDAL GEOMETRY

The question now arises whether the toricity does not change too much the one-dimensional results. Unfortunately, it is not possible to run simply the two-dimensional code ERATO, to detect discrete modes and draw a conclusion as we did in the one-dimensional case. The reason is that all the m's are now coupled through the toricity and, as a consequence, the continuous Alfvén spectrum extends from $\omega^2 = 0$ to $\omega^2 = \infty$. What we can do is to excite the plasma from outside with an antenna and look at the antenna load when varying the applied frequency. Appearing peaks would indicate the existence of discrete Alfvén modes.

It is our intention to prove that the toroidal effects must be

considered for an interpretation of the TCA results (de Chambrier et al., 1981). For this purpose we apply both a cylindrical (Balet et al., 1981) and a toroidal model (Appert et al., 1981) to the equilibrium described by equation (13) and to the TCA parameters used by de Chambrier et al. (1981). In the toroidal version, the TCA antenna is best modelled by a bihelical antenna ($n = 2$, $m = \pm 1$). In the cylindrical version, the antenna load is obtained as a sum of the loads of the two antennae with single helicity. In both cases an artificial damping ν with the value $0.003\ \omega$ has been used. This value is an estimate of the electron Landau damping of the discrete Alfvén waves for the TCA parameters.

The results obtained with the cylindrical model are shown in Fig. 5. The line-averaged density $\bar{n}$, used in Fig. 5, is directly proportional to the previously used dimensionless frequency squared. We find a peak at $\bar{n} = 2 \times 10^{13}\ cm^{-3}$ which is situated just beneath the threshold ($\bar{n}_1$) of the ($n = 2$, $m = 1$) Alfvén continuum. With the value of ν chosen no other peaks (satellites) with the ($n = 2$, $m = 1$)-helicity appear. For higher $\bar{n}$, corresponding to higher ω^2, the antenna load increases rapidly due to the resonant absorption. No further peak appears. This fact is in disagreement with the experiment (de Chambrier et al., 1981).

The results obtained with the toroidal model are shown in Fig. 6. As in the one-dimensional results (Fig. 5) a peak around $\bar{n} \lesssim \bar{n}_1$ can be seen. We find that this peak corresponds to a global Alfvén mode with a dominant $m = 1$ behaviour. With increasing $\bar{n}$, R seems to increase

less rapidly than in the one-dimensional case. However, numerical uncertainty due to poor radial resolution prevents us from drawing a clear curve R ($\bar{n}$) as in the one-dimensional case. Around $\bar{n} \lesssim \bar{n}_2$, which corresponds to the (n = 2, m = 2) Alfvén threshold, a second peak appears. The corresponding mode is global and dominantly m = 2. We therefore conclude that we see the discrete n = 2, m = 2 Alfvén mode which appears due to the toroidal coupling. Qualitatively, the toroidal calculation is in better agreement with the experimental results.

6. IS "DARH" POSSIBLE ?

The resonance phenomena described above could lead to a new heating scheme which we propose to call DARH (Discrete Alfvén Resonance Heating). The efficiency of such a heating scheme is strongly dependent on the answer we can give to a number of questions.

First, we have to know how far the discrete Alfvén wave frequency is from the continuum. The relative distance $\Delta\omega^2/\omega_A^2 = 1-\omega^2/\omega_A^2$ of the discrete Alfvén wave frequency from the lower edge of the continuum is shown in Fig. 7 as a function of the toroidal wavenumber n. We consider the first (uppermost) and the second modes of Fig. 2. One can see that for high n numbers (n > 4) the relative distance $\Delta\omega^2/\omega_A^2 < 1\%$ for the first mode (ℓ = 1) and $\Delta\omega^2/\omega_A^2 < 1\ ^o/oo$ for the second one (ℓ = 2). The smaller is the n number, the larger is the relative distance of the first mode, reaching $\Delta\omega^2/\omega_A^2 = 12\%$ for n = 1 and 55% for n = 0. The second mode develops a local minimum

which disappears when the wall approaches the plasma surface. The relative distance $\Delta\omega^2/\omega_A^2$ = 2% for n = 0. This means that, from the practical point of view, only low-n discrete Alfvén modes can be considered for a DARH heating scheme.

Another important point is the coupling to the antenna which is strongly related to the radial displacement ξ_r of the mode at the plasma surface. In Fig. 8 we display the behaviour of $\xi_r(r)$ of the uppermost mode of Fig. 2 for different n numbers. We can see that this mode behaves as a global kink-like mode for n = 0 (it becomes the unstable kink for n < 0) and becomes more and more internal with increasing n. The arrows, which are marked for n = 0,1,2 and 3, show the radial positions in the plasma where the curve $\omega_A^2(r)$ has its minimum, i.e. where the higher radial modes concentrate (see Fig. 4). The displacement at the plasma surface, which is a measure of the coupling to the antenna, increases as n decreases. For n = 0 it reaches 70% of the maximal displacement.

One of the serious problems of rf heating is that often the energy is deposited close to the plasma surface. Preliminary calculations for DARH using n ≥ 1 show that a large fraction of the power is deposited near to the plasma surface. The situation seems to be similar to that encountered with the usual Alfvén wave heating scheme where the toroidal coupling leads to a certain surface heating (Appert et al., 1981). It therefore appears that DARH using an n ≥ 1 antenna is not advantageous as compared to the resonant absorption. On the other hand, in the case n = 0 DARH has attracting features. The low frequency involved does not appear in any Alfvén continuum. Therefore, there

is no possibility for a coupling to the plasma surface. Since only the cases $n \geq 1$ can be treated with the actual version of our toroidal heating code, we cannot unfortunately corroborate this assertion by a numerical calculation. Another advantageous feature of DARH is the simplicity of an $n = 0$ antenna structure. In the resonant absorption scheme the $n = 0$ antenna is not well coupled to the plasma since the global mode is far from the continuum.

If DARH with the $n = 0$ antenna is to be considered, a frequency tracking is certainly necessary. We know that the $n = 0$ modes are strongly affected by the plasma elongation and by the position of the conducting wall. Small modifications of the plasma surface can change the resonant frequency of the discrete $n = 0$ mode appreciably.

The authors wish to acknowledge the useful discussions with Dr. F. Hofmann, Dr. R. Keller, Dr. J.B. Lister and Dr. A. Pochelon.

This work has been supported by the Ecole Polytechnique Fédérale de Lausanne, by the Swiss National Science Foundation and by Euratom.

REFERENCES

Appert, K., Balet, B., Gruber, R., Troyon, F., Tsunematsu, T. and Vaclavik, J. (1981) Centre de Recherches en Physique des Plasmas, Lausanne, Report LRP 187/81, to be published.

Appert, K., Berger, D., Gruber, R., Troyon, F. and Roberts K.V. (1975) Computer Phys. Commun. 10, 11.

Appert, K., Gruber, R. and Vaclavik, J. (1974) Phys. Fluids 17, 1471.

Balet, B., Appert, K. and Vaclavik, J. (1981) Centre de Recherches en Physique des Plasmas, Lausanne, Report LRP 188/81, to be published.

de Chambrier A. et al. (1981) Centre de Recherches en Physique des Plasmas, Lausanne, Report LRP 195/81, to be published.

Hain, K. and Lüst, R. (1958) Z. Naturforschung 13a, 936.

Newcomb, W.A. (1960) Ann. Phys. (N.Y.) 10, 232.

Pao, Y.P. (1974) Nucl. Fusion 14, 25.

Pochelon, A., Keller, R., Troyon, F. and Gruber, R. (1975) Proc. of 7th Europ. Conf. on Contr. Fusion and Plasma Physics, Lausanne, Vol. I, 157.

References (cont'd)

Ross. D.W., Chen, G.L. and Mahajan, S.M. (1981) Fusion Research Center, Austin, Texas, Report FRCR 227.

Suydam, B.R. (1958) Proc. of the 2nd Int. Conf. on the Peaceful Uses of Atomic Energy 31, 157.

FIGURE CAPTIONS

Fig. 1 Continuous spectrum (hatched region) versus n for a given m. The curves $\omega_A^2(0)$ and $\omega_A^2(1)$ represent the Alfvén frequencies at the axis and at the plasma surface, respectively. The dashed curve is the lower edge of the continuum corresponding to a local Alfvén frequency somewhere inside the plasma (region I). At $n = n_c$ (II), an essential singularity appears at the plasma axis. In region III the lower edge of the Alfvén continuum is determined by $\omega_A^2(0)$.

Fig. 2 : Spectrum of the discrete Alfvén modes for the standard case. The distance $\Delta\omega^2$ from the lower edge of the Alfvén continuum is plotted versus the toroidal wavenumber n. For negative n's the uppermost kink-like mode turns unstable. In the whole range $-.12 < n < 7.28$ there is an accumulation point at $\Delta\omega^2 = 0$. The highest density of the discrete modes occurs at $n = n_c$.

Fig. 3 : Distance $\Delta\omega^2$ at $n = n_c$ versus the radial mode number ℓ. For $\ell \geq 10$, $\Delta\omega^2 \sim 1/\ell^4$ as predicted by the WKB analysis.

Fig. 4 : Radial displacement ξ_r as a function of radius for different radial mode numbers. In 4a, the lowest 4 modes are plotted for n = 2 (region I); in 4b, the lowest 6 modes at the essential singularity point (II) and in 4c, the lowest 4 modes at n = 4 (region III) are shown. The arrow in 4a shows the position at which $d\omega_A^2/dr = 0$.

Figure captions (cont'd)

Fig. 5 : Antenna load R versus line-averaged density as obtained with the cylindrical model evaluated for a deuterium plasma embedded in a 1.2T toroidal field and acted upon with a frequency of 2.67 MHz. The load seen by the whole antenna structure is given by 8R. The threshold density $\bar{n}_1$ corresponds to the minimum $\bar{n}$ for which the Alfvén resonance with the helicity (n = 2, m = 1) is situated in the plasma.

Fig. 6 : Antenna load R versus line-averaged density as obtained with the toroidal model. The equilibrium and the excitation frequency are the same as for Fig. 5. The threshold densities $\bar{n}_1$ and $\bar{n}_2$ correspond to the onset of the continua (n = 2, m = 1) and (n = 2, m = 2), respectively.

Fig. 7 : Relative distance $\Delta\omega^2/\omega_A^2$ from the lower edge of the Alfvén continuum for the first two radial modes versus n.

Fig. 8 : Radial structures of ξ_r of the first discrete Alfvén mode for different values of n. The arrows show the radial positions where the curve $\omega_A^2(r)$ has its minimum.

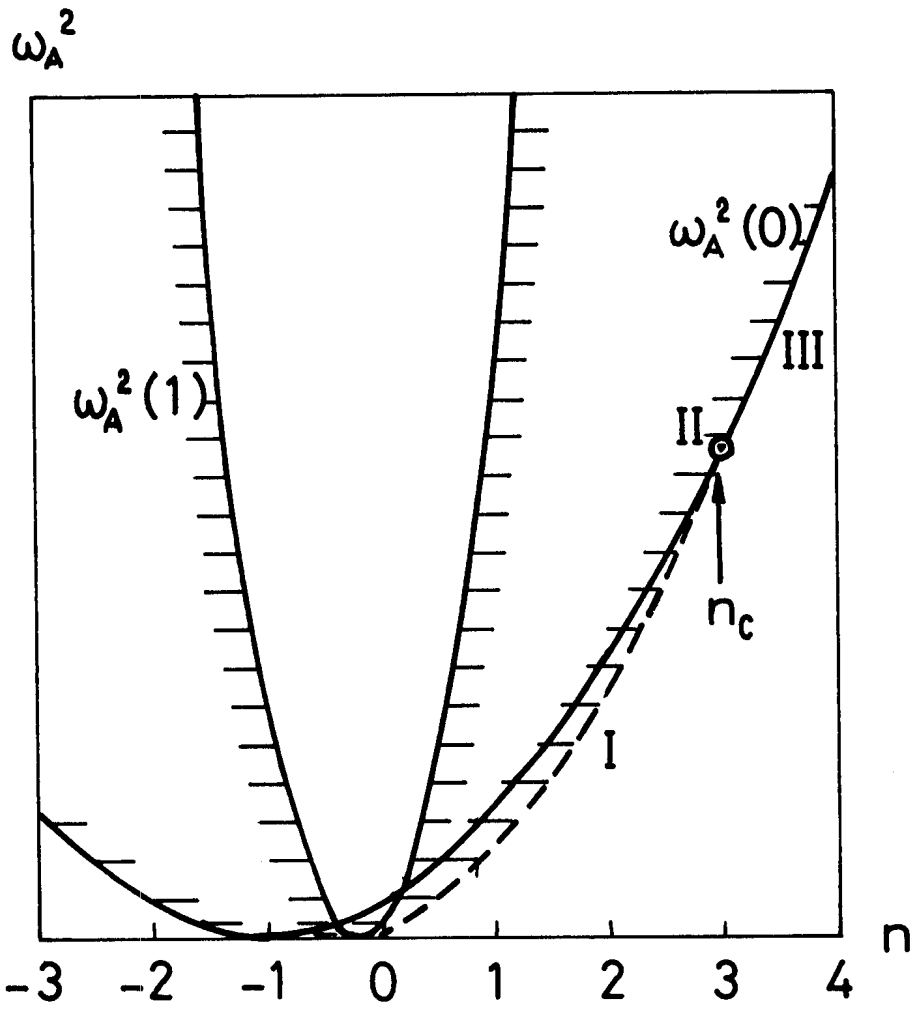

FIG. 1

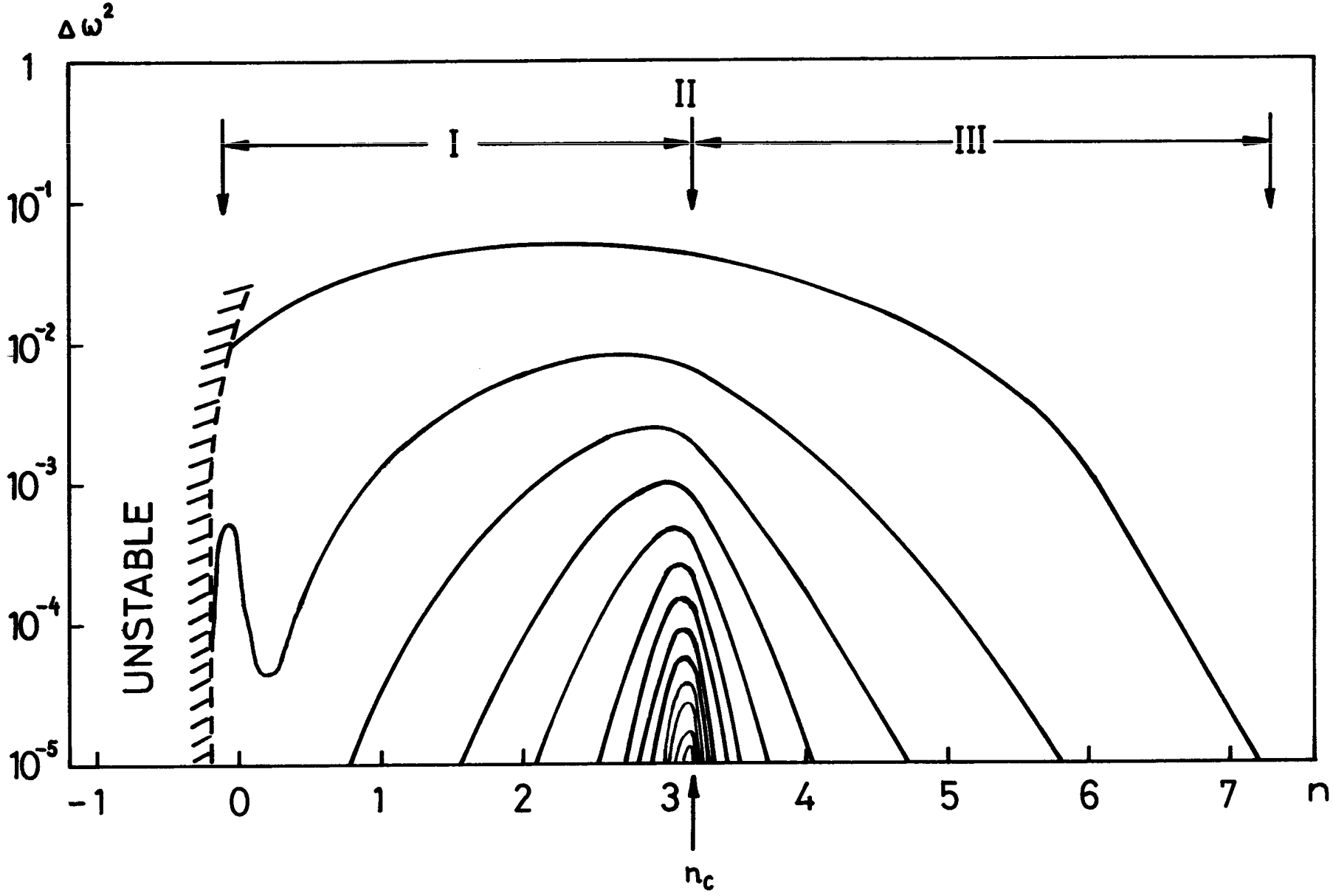

FIG. 2

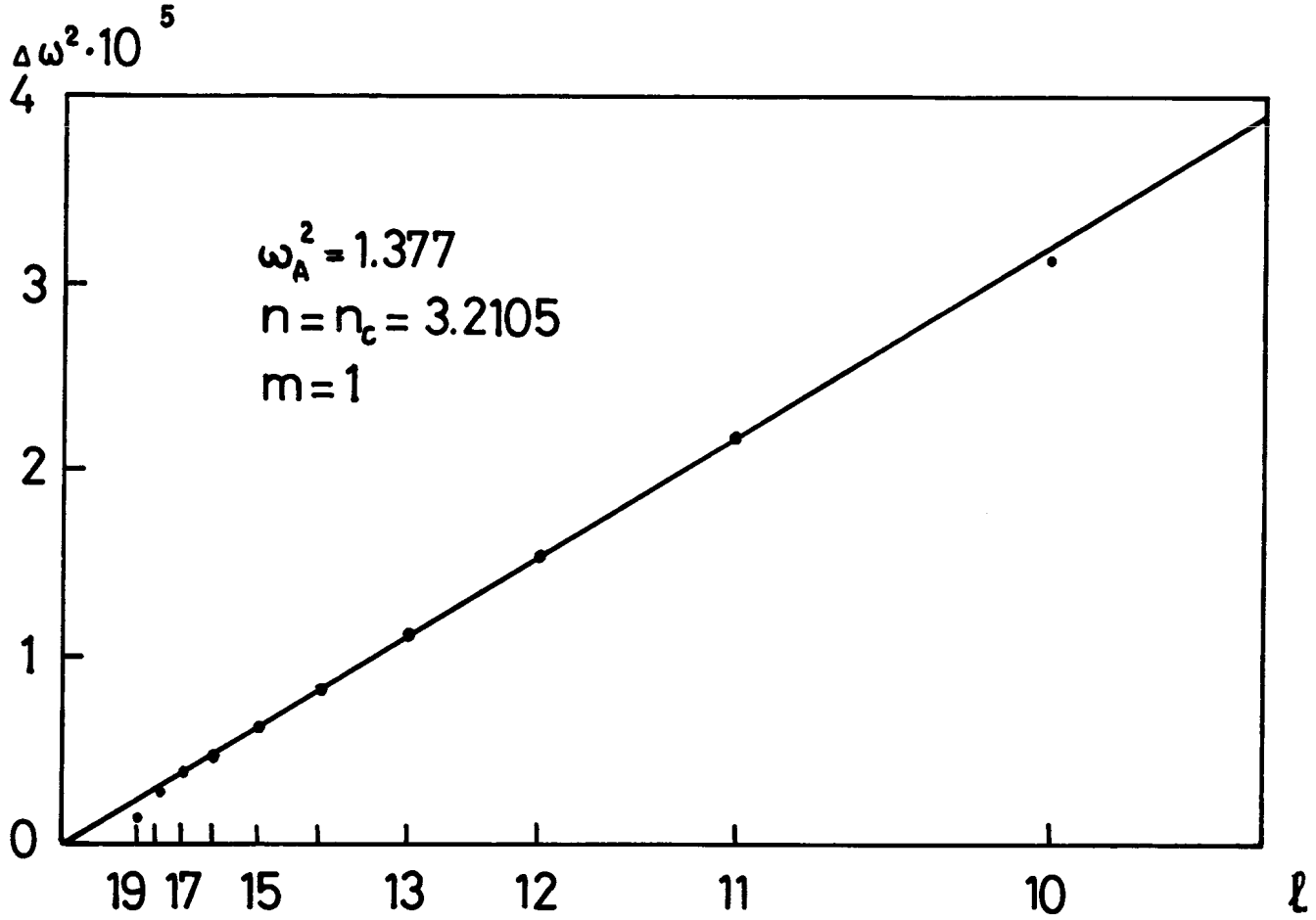
$\Delta\omega^2 \cdot 10^5$
4
3
2
1
0
$\omega_A^2 = 1.377$
$n = n_c = 3.2105$
$m = 1$
19 17 15 13 12 11 10
ℓ

FIG. 3

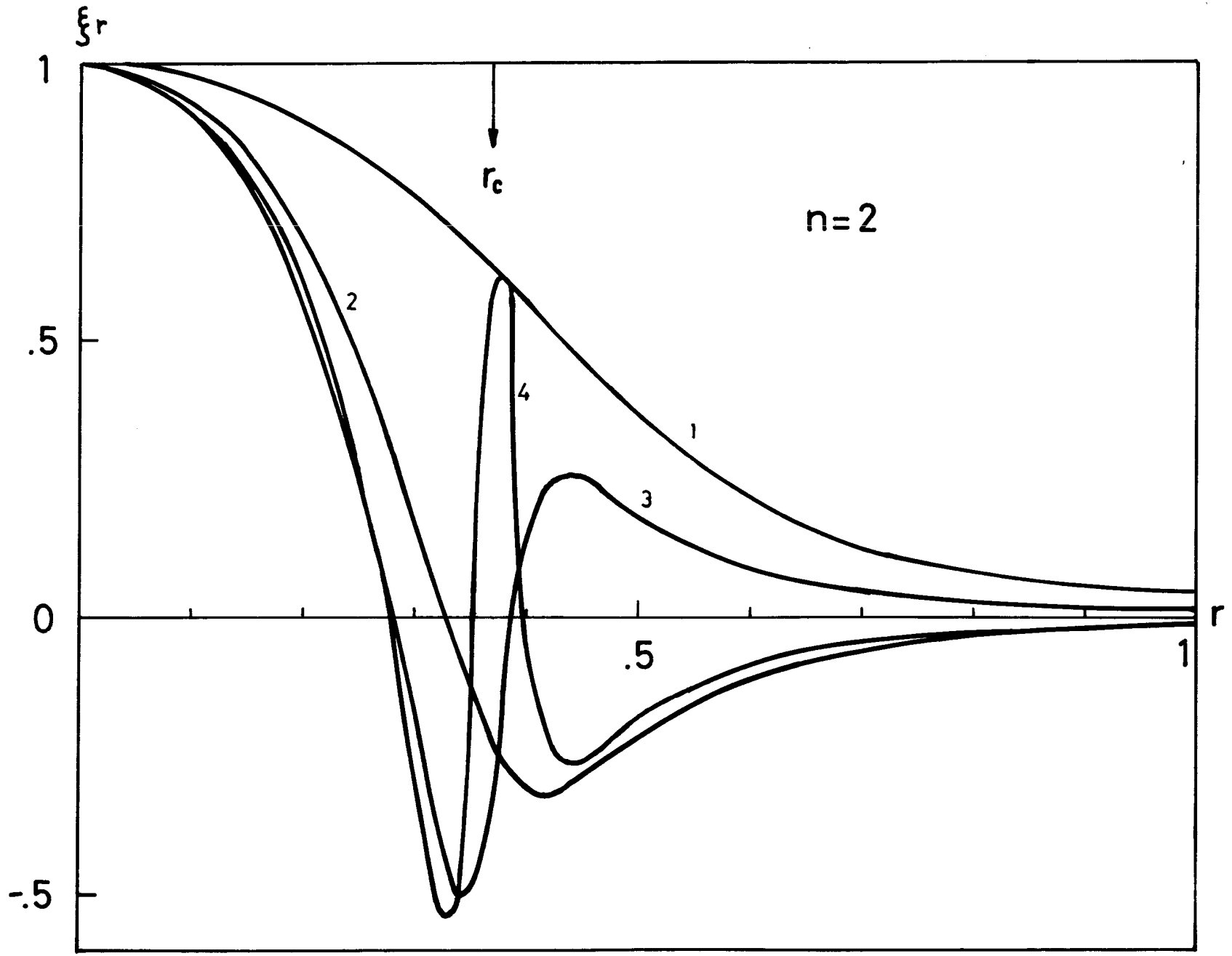

FIG. 4A

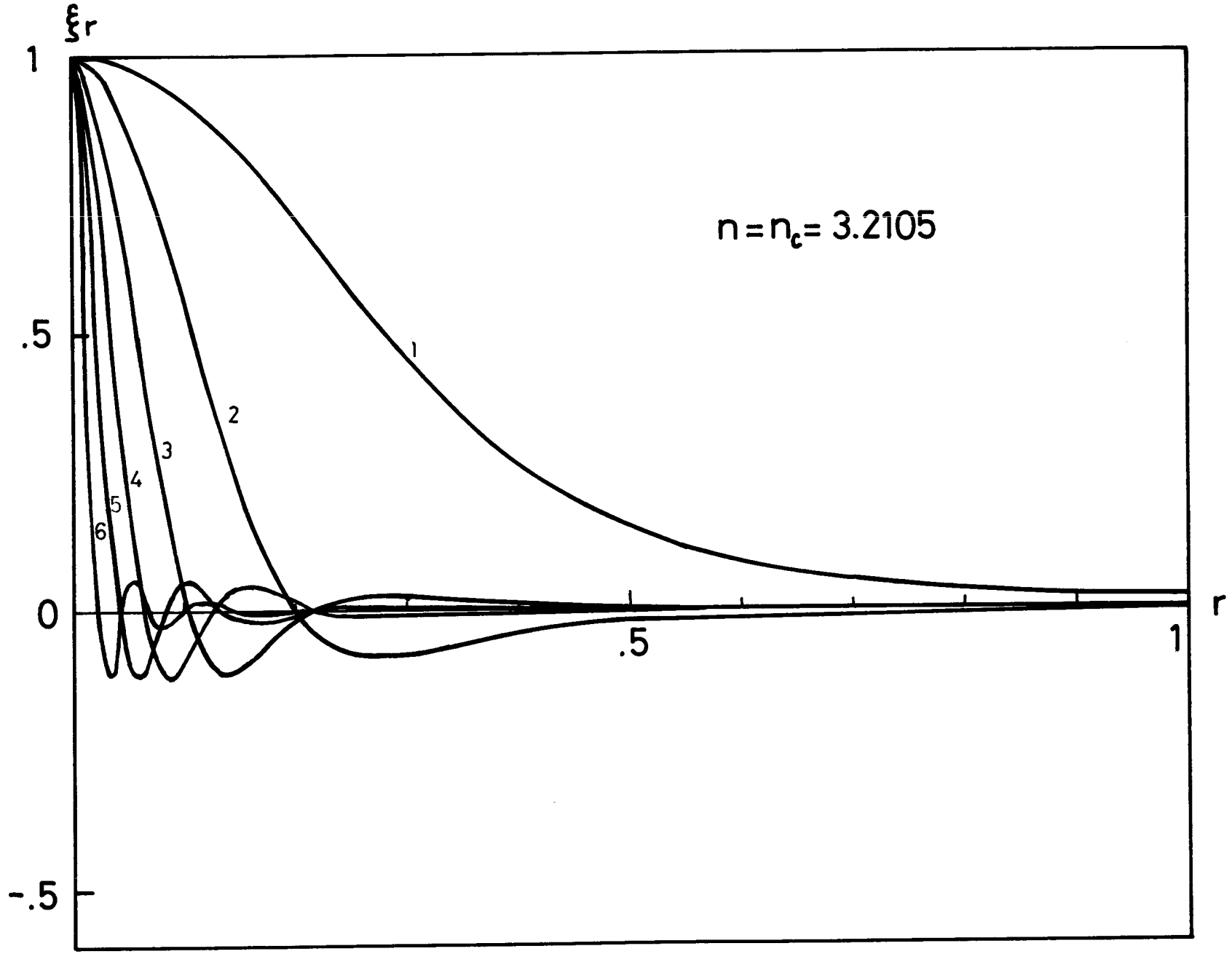

FIG. 4B

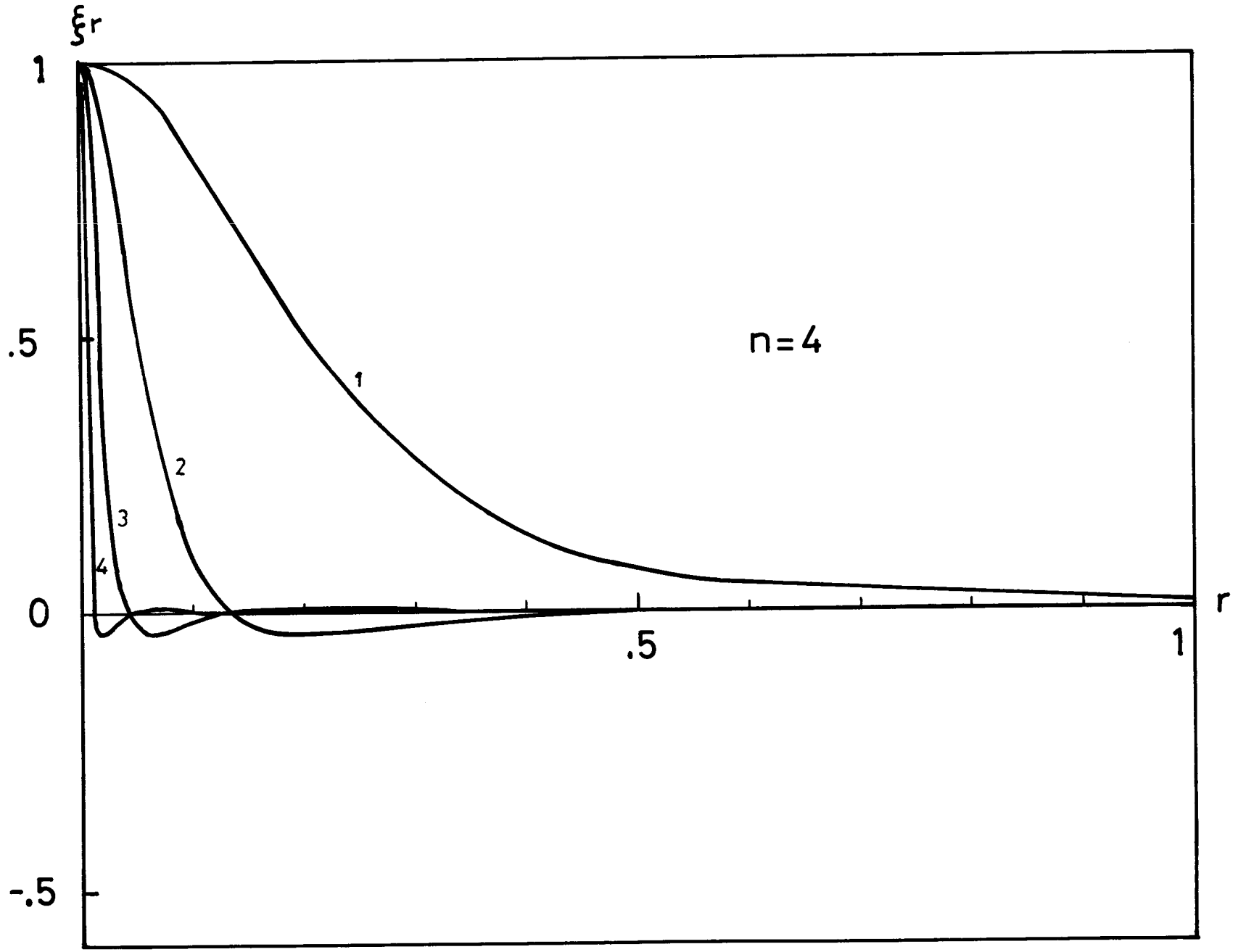

FIG. 4 C

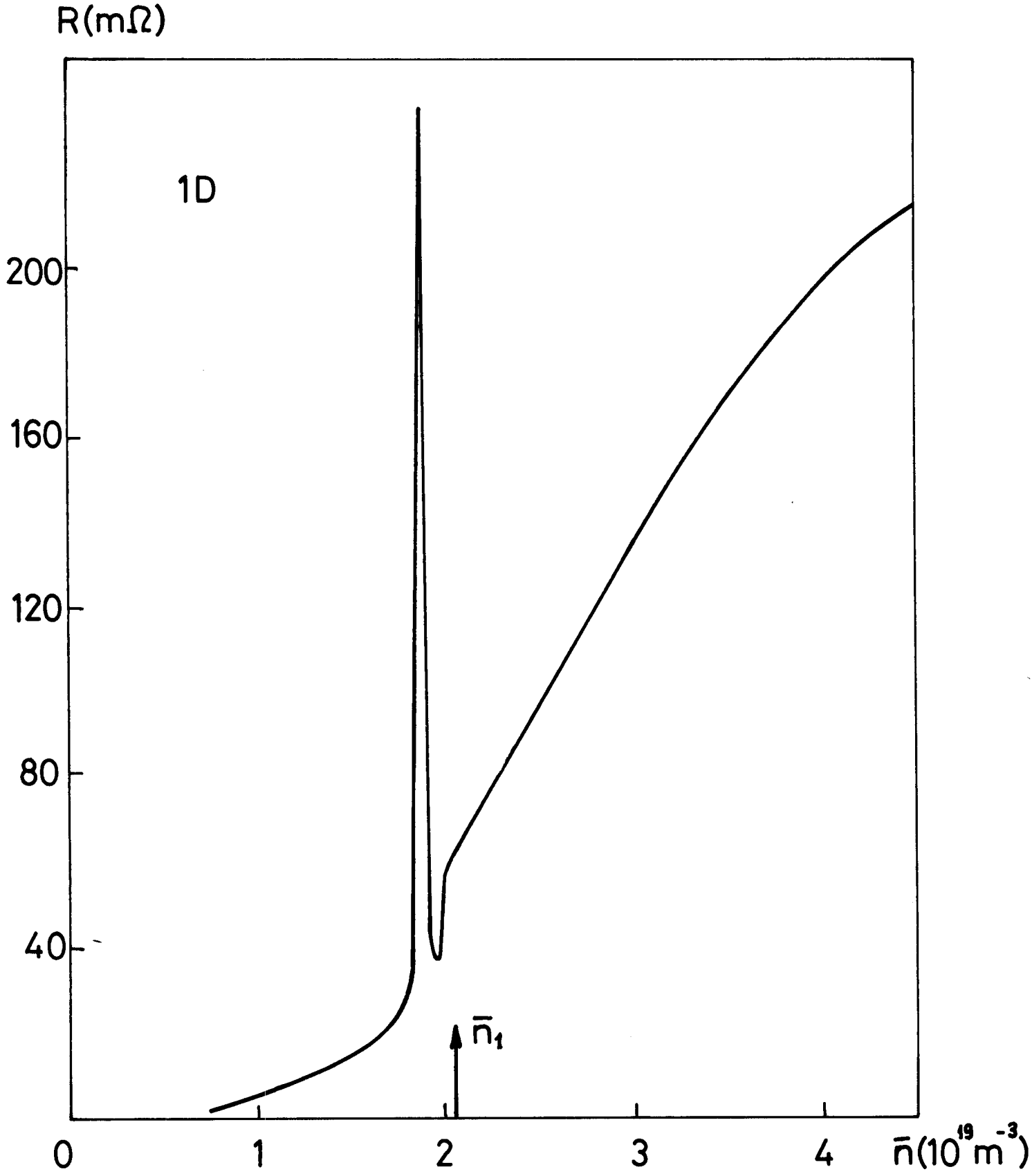

FIG. 5

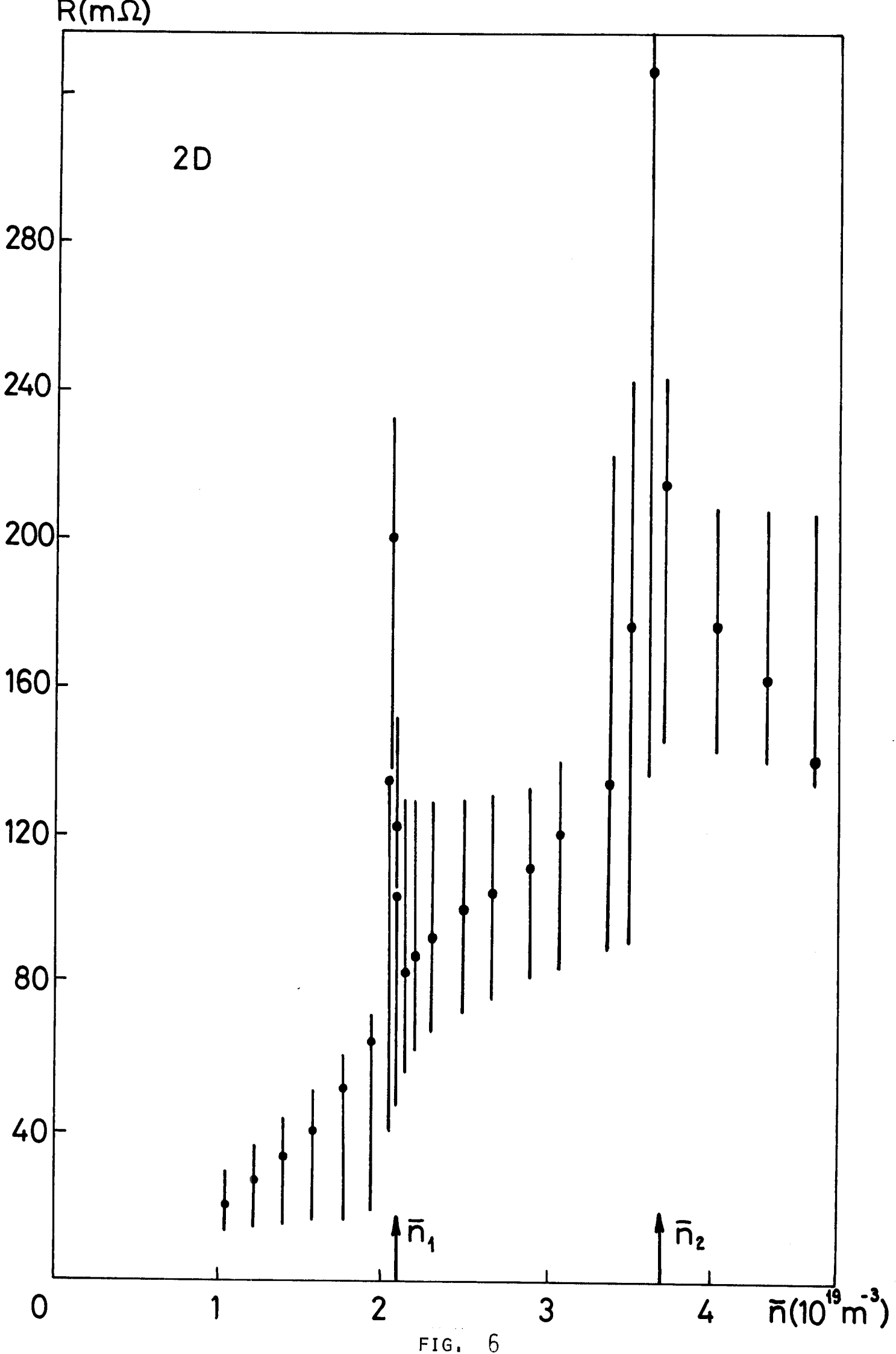

FIG. 6

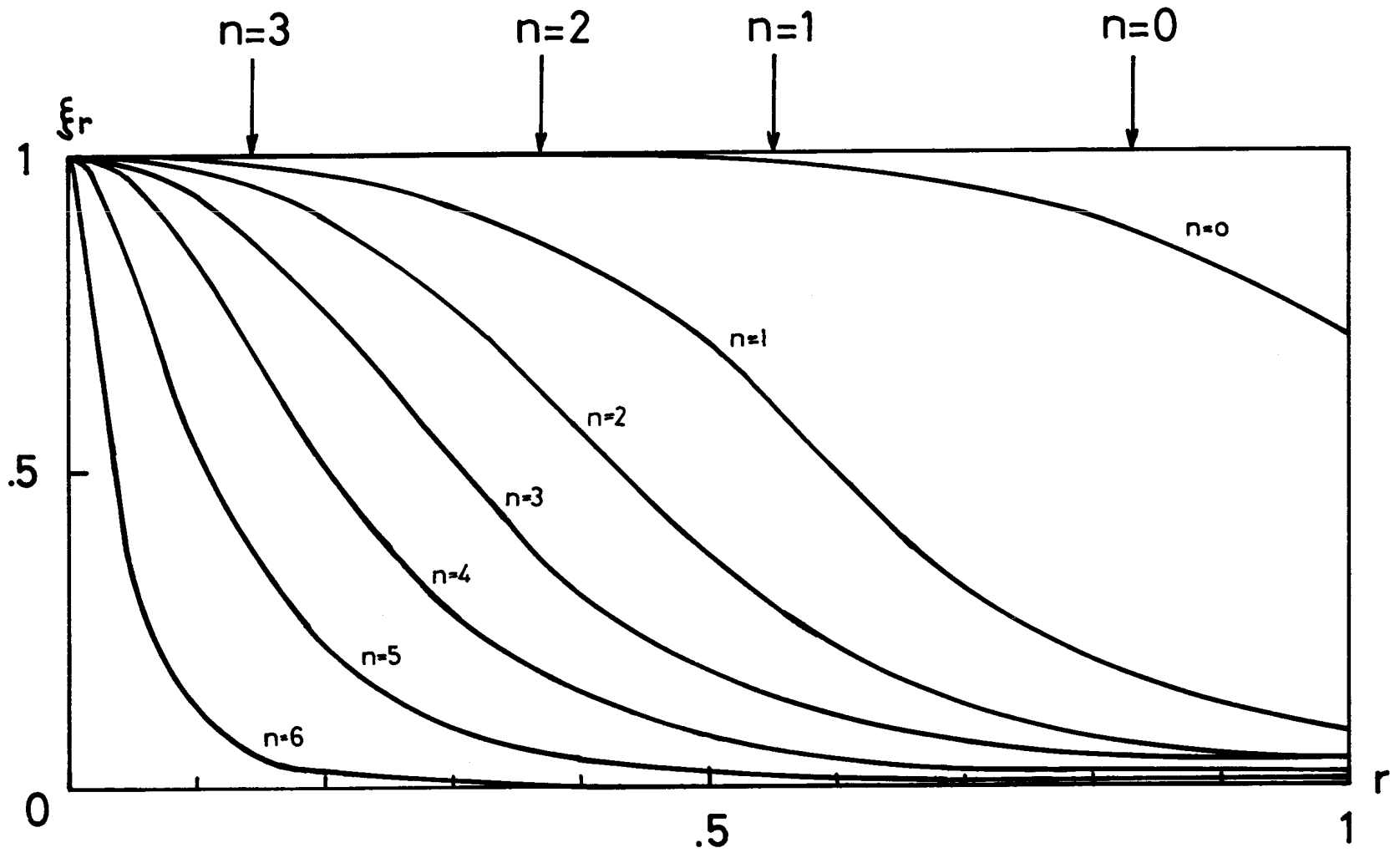

FIG. 8